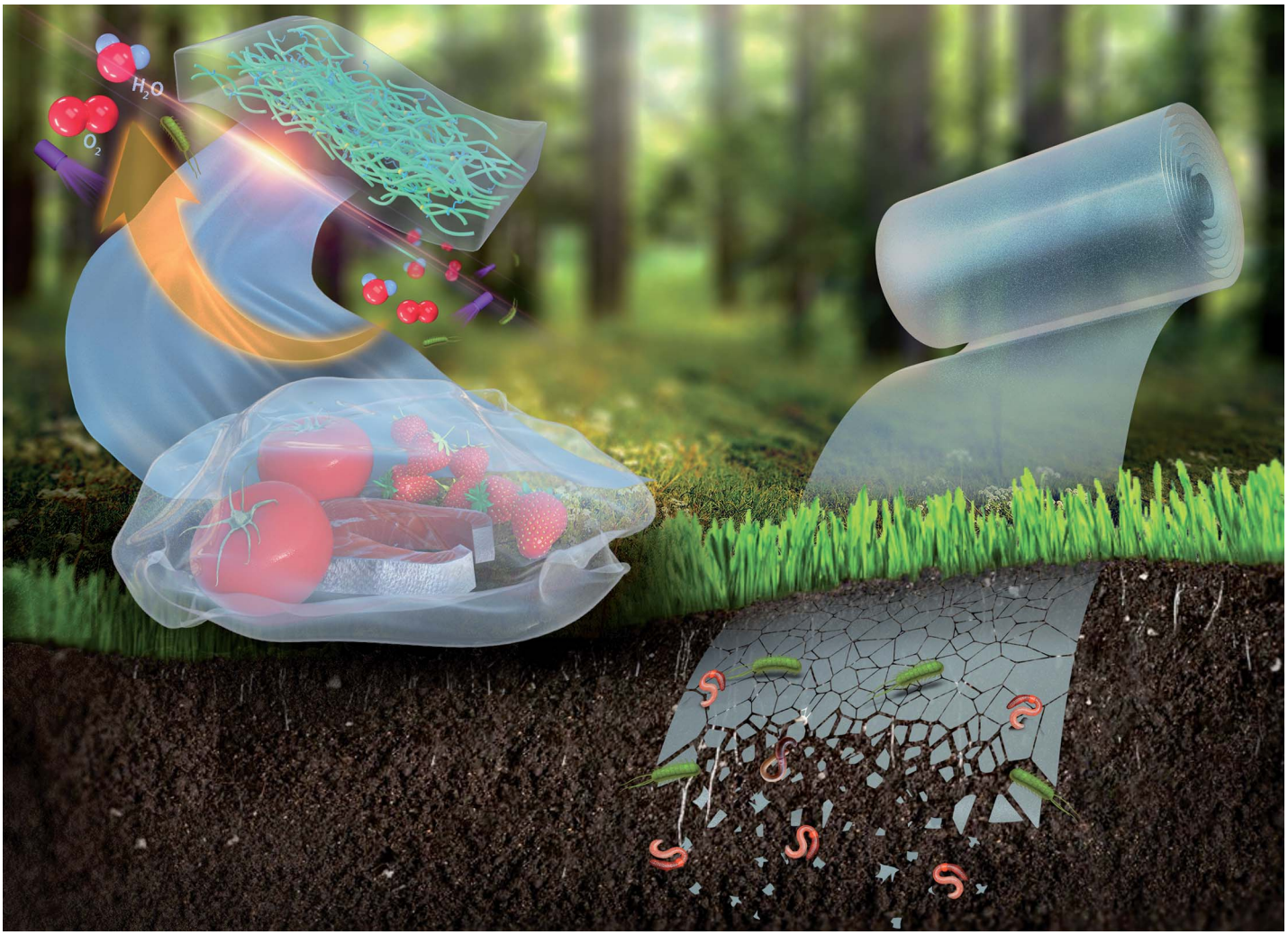

Showcasing research from Professor To Ngai's laboratory, Department of Chemistry, Chinese University of Hong Kong, Sha Tin, N.T., Hong Kong.

Development of strong and high-barrier food packaging films from cyclic-anhydride modified bacterial cellulose

Using non-substituted and long-chain substituted cyclic anhydrides as the esterifying agents, this work reports simple, efficient, and low-pollution surface modification protocol to fabricate BC films with good mechanical and water vapor, oxygen, and foodborne pathogenic bacterial barrier properties. The fabricated films also show visible improvement in thermal stability and are biodegradable within one month in soil. They thus have high potential in replacement of widely used petrochemical plastic-based food packaging materials.
Image credit: To Ngai

As featured in:

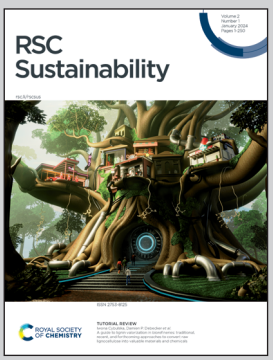

See To Ngai *et al.*,
RSC. Sustainability., 2024, **2**, 139.

ROYAL SOCIETY OF CHEMISTRY

rsc.li/rscsus

Registered charity number: 207890

RSC Sustainability

ROYAL SOCIETY OF CHEMISTRY

PAPER

View Article Online
View Journal | View Issue

Cite this: *RSC Sustainability*, 2024, **2**, 139

Development of strong and high-barrier food packaging films from cyclic-anhydride modified bacterial cellulose†

Zhuolun Jiang, Ka Man Cheung and To Ngai *

Using non-substituted and long-chain substituted cyclic anhydrides as the esterifying agents and dimethyl sulfoxide as the solvent, high water vapor/oxygen/bacterial resistant, mechanically/thermally strong, and biodegradable bacterial cellulose (BC) films have been fabricated according to a simple, efficient, and low-pollution surface modification protocol. The anhydride loading, reaction time and characterization in terms of the esterification degree, crystallinity, microstructures, transparency, barrier resistance, mechanical and thermal properties of the films, and fruit preservation tests were investigated. Modification with 10 wt% dodecenyl succinic anhydride (DSA) increased the dry tensile strength (TS) of the film to 124 MPa and the wet TS to 81 MPa in 30 min. Modification with 10 wt% octadecenyl succinic anhydride (OSA) reduced the water vapor permeability of the film by 84% and yielded the highest antimicrobial effect on the film surface. The film modified with 3 wt% of maleic anhydride (MA) had the strongest oxygen barrier and preserved strawberries most effectively. These films were totally biodegraded in soil within one month and exhibit strong potential to be bio-based and biodegradable food packaging materials.

Received 2nd July 2023
Accepted 19th October 2023

DOI: 10.1039/d3su00219e

rsc.li/rscsus

Sustainability spotlight

Petroleum-based plastic films have been used extensively in food packaging. However, the most widely used plastics produce large amounts of nondegradable waste pollutants. In recent years, bacterial cellulose (BC) has gained increasing attention as an alternative to plastic packaging because of its renewability, biodegradability, and non-toxicity. However, due to the abundant hydroxyl groups (–OHs) on the polymer chains, BC films show high hydrophilicity, and humid conditions greatly reduce the strength and barrier properties of the films. Using cyclic anhydrides as the acylants and DMSO as the solvent, we developed a simple, efficient, and low-pollution surface modification protocol to fabricate BC films with good mechanical and water vapor, oxygen, and foodborne pathogenic bacterial barrier properties. Furthermore, all of the anhydride-modified films showed visible improvements in thermal stability by around 32 °C and good biodegradation rate (100% biodegradation in 1 month) in soil. We believe that those biobased films display high potential in replacement of the widely used petrochemical plastic-based food packaging materials as high water and oxygen vapor barrier, strong and biodegradable films to greatly extend shelf-lives of foods and effectively relieve the white pollution in the environment.

Introduction

Synthetic petrochemical-derived plastic packaging has provided tremendous convenience in human's daily life due to its low cost, light weight, and good mechanical strength; however, intense concerns have been raised regarding the associated enormous consumption of fossil fuel resources and adverse ecosystem effects of these non-biodegradable materials.[1,2] In the past several decades, increasing attention has been paid toward exploiting sustainable, low-cost, strong, and biodegradable food packaging, and natural resources such as polysaccharides and proteins have been highlighted.[3–5] Cellulose is a water non-soluble polysaccharide found widely in the cell walls of plants and microorganisms, and has a linear structure composed of repeating β-1,4-linked D-anhydroglucose units. For more than a century, cellulose has been a popular component of applications in numerous fields, including cosmetics, pharmaceuticals, electronic devices, packaging, emulsion, and water treatment.[3,6–13] The bacterial cellulose (BC) is a bacteria-derived cellulose material most effectively secreted by the non-pathogenic bacteria *Komagataeibacter xylinus*. This material features high chemical purity (without lignin, hemicellulose, and pectin), non-toxicity, and an interconnected ultrafine three-dimensional (3D) structure.[12,14] Compared with the production of plant cellulose films, the production of BC films or suspension is greatly simplified, and the films display superior strength and flexibility.[12,15] However, due to the abundant hydroxyl groups (–OHs) on the polymer chains, BC films show high hydrophilicity, and humid conditions greatly reduce the

Department of Chemistry, The Chinese University of Hong Kong (CUHK), Shatin, NT, Hong Kong, China. E-mail: tongai@cuhk.edu.hk

† Electronic supplementary information (ESI) available. See DOI: https://doi.org/10.1039/d3su00219e

strength and barrier properties of the films, including the water vapor and oxygen barriers. These changes can sharply reduce the shelf-lives of oxygen-sensitive packaged foods such as strawberries and meats due to the accelerated loss of moisture and proliferation of microorganisms.[16,17] However, these –OHs also enable chemical functionalization of cellulose (*e.g.*, esterification, silylation, etherification, amidation), which confers new properties upon the BC films and thus paves the way for multiple practical applications in areas such as food and biomedicine.[18,19]

Some studies have reported methods of hydrophobic modification such as coating or blending of hydrophobic agents with a hydrophilic cellulose substrate,[20–23] or chemically modifying cellulose nanofibers/nanocrystals using esterifying agents (acylants) in the presence of an organic solvent. However, these approaches have led to problems such as decreases in the transparency, smoothness, flexibility, biodegradability, and mechanical and thermal properties of the films, and the consumption of large volumes of organic solvents (*e.g.*, ionic liquids, *N*,*N*-dimethylacetamide/lithium chloride) during the cellulose fiber dissolution, solvent exchange, and precipitation/purification steps.[24–30] 2-Octenylsuccinic anhydride (OSA) has been used to modify starch for use as a common, safe food additive for years.[31,32] In our previous study, we conducted esterification using dimethyl sulfoxide (DMSO) as a pre-swelling solvent to activate the –OHs of BC films and three types of long-chain anhydrides as the hydrophobic modifiers, including OSA to hydrophobically modify the BC film surface, fabricating BC films with significantly promoted mechanical and barrier properties. The resultant OSA-modified BC films displayed the highest water vapor/antimicrobial resistance and mechanical/thermal properties. However, they exhibited a low biodegradation rate in a natural environment as OSA, which bears the shortest substituted chain, has the highest grafting degree and crosslinking capability when compared with longer-chain dodecenyl- (DSA) and octadecenyl-succinic anhydride (ODSA).[11,32] As a result, as a follow-up of our previous work, in this study, a cyclic anhydride with a shorter substituted group, typically, maleic anhydride (MA), will be attempted to investigate whether grafting a shorter substituted chain to the BC surface could achieve better results, *e.g.*, better water/water vapor resistance and higher crosslinking degree. In the present study, premade BC films were immersed in DMSO containing anhydrides in various ratios to compare the esterification and crosslinking capabilities of a non-substituted cyclic anhydride, namely MA, with those of long-chain alkenyl succinic anhydrides, including OSA, DSA, and ODSA. The anhydride ratio and reaction duration were initially adjusted, during which the reaction medium could be recycled and reused with appropriate solvent and acylant supplementation due to the cyclic structure of the acylant, which prevented the production of acid byproducts in the reaction medium.[33] The reaction degree, film micro- and crystalline structures, barrier, mechanical/thermal, fruit preservation and biodegradation properties of the modified films were also explored in this work.

Experimental section

Materials

A never-dried alkali-purified, aqueous BC suspension (0.8 wt%; source: *Komagataeibacter*; fiber size: 50–100 nm in diameter, 20 μm in length) was supplied by Qihong Technology (Guilin, China). Low-density polyethylene (LDPE) films (thickness: 20 μm) were obtained from the local supermarket. MA (98%) was obtained from Alfa Aesar (Thermo Fisher Scientific, USA). OSA (95.0%; a mixture of *cis*- and *trans*-isomers), DSA (90.0%; a mixture of branched-chain isomers), and ODSA (93.0%; a mixture of isomers) were obtained from Macklin (Shanghai, China). Absolute ethanol (AR grade; VWR, Fontenay-Les-Bois, France) and deionized (DI) water (Milli-Q grade, 18.2 MΩ cm) were used for purification. DMSO (GR grade; Duksan, South Korea) was used without further purification.

Preparation of BC films

BC films were fabricated by solvent casting according to our reported method.[16] The resulting dry BC films were carefully peeled from the dishes and stored in sealed LDPE bags at room temperature (RT) under natural light. The thickness of each film was measured at 10 random points using a digital micrometer accurate to 0.001 mm, which revealed that the average film thickness was approximately 40 μm. There were no significant differences in thickness between the BC films modified using different anhydrides (*i.e.*, MA, OSA, DSA, and ODSA).

Esterification of BC films

A circular BC film (diameter: 8 cm) was divided into four pieces with identical widths (2 cm), which were soaked in a reaction medium consisting of DMSO (20 g) and various anhydride ratios (w/w) at 70 °C to react statically for different durations. At various time intervals (10 min, 30 min, 1 h, and 3 h), one film strip was withdrawn and, washed once with absolute ethanol and DI water in sequence *via* ultrasonication (37 kHz, 100% power; 5 min for each washing step) to remove DMSO and unreacted anhydride on the film surface. The film was then air-dried in an oven at 60 °C for 24 h and stored at RT. The MA-, OSA-, DSA-, and ODSA-modified BC films were named C0-BC, C8-BC, C12-BC, and C18-BC, respectively, according to the carbon atom number of the substituted chain linked to the cyclic structure of the anhydride.

Determination of mechanical properties

The mechanical properties of the films were determined by stress–strain tests using a universal tensile testing machine (TOHNICHI, Zhuoyue, Dongguan, China). The ultimate tensile strength (TS) and elongation at break (EAB) were calculated according to eqn (1) and (2):[34]

$$\mathrm{TS} = F/\mathrm{A} \quad (1)$$

$$\mathrm{EAB} = \Delta L/L \quad (2)$$

where F is the maximum force at the rupture point (N); A is the film cross-sectional area (m^2); ΔL is the increase in length before breakage (m); and L is the initial length between the grips (m). These measurements were performed in triplicate, and the averages and standard deviations are reported.

Fourier-transform infrared (FTIR) spectroscopy

The chemical structures of the films were identified using FTIR spectroscopy (Nicolet iS10, Thermo Scientific, USA) in the range of 4000–400 cm^{-1}. Each film was scanned 32 times at a resolution of 4 cm^{-1} in transmission mode.

Film microstructural and elemental analysis

Scanning electron microscopy (SEM; JSM-7800F, JEOL, Tokyo) and energy dispersive X-ray spectroscopy (EDS) were used to characterize the microstructure and chemical compositions of the obtained films. SEM micrographs of the coated films were taken at 5000×, 20 000×, and 100 000× magnification to observe the surface and cross-section morphology. The degree of surface substitution (DSS; molar ratio of the grafted anhydride to anhydroglucosidic units of BC) of each sample was calculated from the EDS results and the atomic weight (awt%) of carbon in the detected region. Three locations were tested in each sample, and the chemical composition of each film is presented as the mean ± standard deviation.

X-ray diffraction (XRD)

The XRD patterns of the BC films were obtained using a diffractometer (Rigaku SmartLab 9 kW, Japan) at 40 kV and 80 mA. The scans were conducted at 25 °C over the range of 10–50° (2θ), with a ramping rate of 10° min^{-1}. The crystallinity index (CrI) was calculated from the XRD diagrams according to eqn (3):[35]

$$\mathrm{CrI} = (I_{22.8^\circ} - I_{18.3^\circ})/I_{22.8^\circ} \quad (3)$$

where $I_{22.8^\circ}$ is the maximum intensity of the largest crystal plane reflection of a sample, and $I_{18.3^\circ}$ is the maximum intensity of the X-ray scattering broadband caused by the amorphous part of a sample.

Water contact angle (WCA) analysis

The hydrophobicity of the fabricated BC films was determined using a contact angle measurement instrument and analyzed using SCA20 software (OCA 25, Dataphysics Company, Germany) with the "sessile drop" method.[20] The test was performed in quadruplicate on each film, and the averages ± standard deviations at 1 min and 5 min are reported.

Water swelling (WS) ratio

The WS ratio of the modified BC films was calculated using eqn (4), according to our reported method:[16]

$$\mathrm{WS} = (M_1 - M_2)/M_2 \quad (4)$$

where M_1 is the weight of a sample after wiping, and M_2 is the weight of a sample after preconditioning in an oven at 60 °C for 5 h. These measurements were performed in triplicate, and the averages ± standard deviations are reported.

Water vapor permeability (WVP)

The WVP of the films was calculated according to our previous study,[16] using a constant temperature and relative humidity (RH) chamber (SUNNE, Shangpu Instrument Equipment, Shanghai, China). Tests were performed at an RH of 75% and temperature of 30 °C for 24 h. The weights of the bottles were recorded 4 h and plotted against time, and the slope of the resulting curve was determined using linear regression. The WVP was then calculated using eqn (5):[36]

$$\mathrm{WVP} = (\Delta m \times d)/(A \times \Delta t \times \Delta P) \quad (5)$$

where Δm, Δt, A, and d represent the weight difference (g), time interval (h), film coverage area (m^2) and film thickness (m), respectively, and ΔP indicates the WVP difference (Pa) between the two sides of the film, which is 3182.3 Pa at 75% RH and 30 °C. These measurements were performed in triplicate, and the averages ± standard deviations are reported.

Thermal properties

The maximum decomposition temperature (T_{max}, the temperature at which the y-axis value of the differential thermogravimetry (DTG) curve was lowest) was determined using a thermogravimetric analyzer (TGA-6, PerkinElmer, USA). In the thermal analysis, each film sample (approximate weight, 5 mg) was heated from 30 °C to 650 °C at a rate of 10 °C min^{-1} under a nitrogen flow at a rate of 20 mL min^{-1}.

Antimicrobial properties

The antimicrobial test was conducted according to our previous method, using *S. aureus* and a modified strain of *E. coli* that constitutively expresses green fluorescent protein, which were visible as dark and white dots, respectively, *via* microscopy.[16] Phase contrast and epifluorescence microscopes were used to observe the distribution of bacteria on the film surfaces according to the areas of dark or white regions. These measurements were performed in triplicate.

Oxygen barrier properties

The oxygen barrier properties were determined using our reported strategy with reduced iron powder as the oxidant using the weight method.[16,37] The tests were performed at 30 °C and an RH of 95% for 24 h. The weights of the bottles were recorded every 4 h and plotted against time, and the slope of the resulting curve was determined using linear regression. The oxygen transmittance rate (OTR) was calculated using eqn (6):

$$\mathrm{OTR} = \Delta m/(A \times \Delta t) \quad (6)$$

where Δm and A represent the weight difference (g) and the film covering area (m^2), respectively; and Δt denotes the time interval.

These measurements were performed in triplicate, and the averages ± standard deviations are reported.

Transparency and ultraviolet barrier properties

The ultraviolet-visible (UV-vis) spectra of the films at 200–800 nm were obtained using a UV-vis-near infrared spectrophotometer (UV-3600 Plus, Shimadzu, Japan) in the transmission mode.

Changes in strawberry quality during storage

Fresh strawberries were purchased from a local market. The strawberry preservation test was conducted according to our reported method, which involved observing the appearance of strawberries packed in containers that had been covered or not with the films and stored for 7 d in a refrigerator (4 °C, 40% RH) or 2 d at RT.[16] A LDPE food wrapping film was used as the control. The weight loss ratio of the packaged strawberries after 7 d in the refrigerator was determined using the weight method, and measurements were taken three times to appraise the preservation effectiveness of the films.

Biodegradation test

The biodegradation capacity of the films was tested by burying them in natural soil at a depth of 10 cm for 10–30 d.[16,38] After 10 d, the film fragments were removed from the soil, rinsed with water, and dried in an oven, and the weight loss ratio was determined using the gravimetric method and characterized by FTIR spectroscopy. Then the tested films were re-buried in soil at a depth of 10 cm for 20 d to observe the biodegradation situation.

Results and discussion

Fig. 1 depicts the explicit mechanism of acylation between the cyclic anhydride and –OHs on BC, with the solvent DMSO also providing strengthening (Table 1) and catalytic functions. The DMSO treated film reached the optimal TS at 5 min,[16] which might be explained by the convergence of fibers at the surface that developed strong bonds and made the film much smoother, denser, and stronger than the original state.[16,39] The gradually decreasing TS of the DMSO treated film from 10 min to 3 h could be explained by the increasing thickness of the regeneration region that destroyed the inner hydrogen bonding and supramolecular structure of the BC fibers.[27,40] The lone pairs of electrons on DMSO can coordinate with the succinyl ring of the anhydride to form an intermediate, thus facilitating the reaction of the anhydride with the –OHs of BC.[32]

Table 1 Mechanical strength of the pristine BC and DMSO treated BC films (1–60 min, 70 °C) in the dry state

Time	TS (MPa)	EAB (%)
0	28.2 ± 1.5	13.6 ± 0.1
5 min	114.3 ± 3.8	18.2 ± 1.1
10 min	106.4 ± 4.2	14.2 ± 0.7
30 min	84.1 ± 2.1	12.0 ± 0.6
1 h	86.5 ± 1.9	11.9 ± 0.5
3 h	72.6 ± 1.6	8.8 ± 0.7

Optimal ratio of the anhydride in DSMO

Introducing hydrophobic alkyl groups onto BC decreases the hydrophilicity, therefore increasing the wet TS of the films.[41] Initially, anhydride in DMSO at ratios of 1% to 20% was loaded for the surface modification of the BC film at 70 °C for 5 min. The optimal mechanical film strength was achieved at 3% MA, 5% OSA, 10% DSA, and 15% ODSA (Table S1† and Fig. 2), indicating that the longer the substituted chain, the lower the anhydride reactivity.[42] The similarly high reactivities of 5% OSA and 3% MA revealed that the reactivity of OSA was significantly higher than that of the other two long-chain anhydrides (DSA and ODSA), which required loading ratios of 10–15% due to their stronger steric hindrance.

Degree of surface substitution (DSS)

In the following experiments, the films were modified with anhydride for 10 min to 3 h at the optimal ratio of each anhydride in DMSO. The DSS value of each film is reported (Table 2) according to quantitative EDS analysis of the awt% of carbon at the BC film surface (Table S2†). For 3% C0-BC, a DSS of 3 was reached in only 10 min, revealing the ultrahigh reactivity of MA, while the DSS of 5% C8-BC, 10% C12-BC, and 15% C18-BC gradually increased during this period. 5% C8-BC reached a higher DSS (0.19) than 10% C12-BC (0.1) or 15% C18-BC (0.12) at 3 h due to the shorter alkenyl chain on OSA, which exhibited higher reactivity with BC.

Mechanical properties

Influenced by surface regeneration, esterification, crosslinking, and some side interactions (*e.g.*, solvent over-swelling and transesterification), the modified films during 10 min to 3 h exhibited increasing and fluctuating trends in mechanical strength, as displayed in Table S3† and Fig. 3.[16] Although the

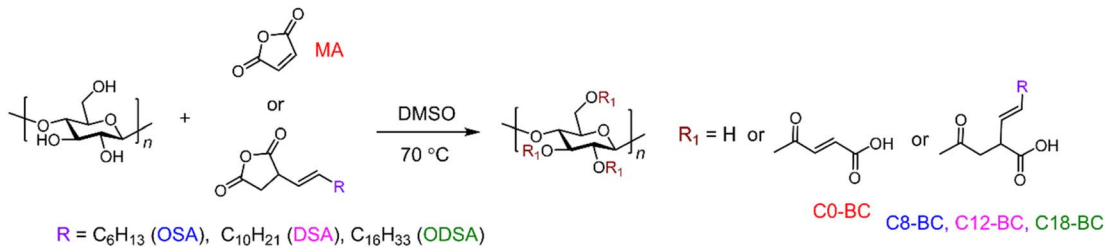

Fig. 1 Schematic illustration of esterification between BC and anhydrides in DMSO at 70 °C.

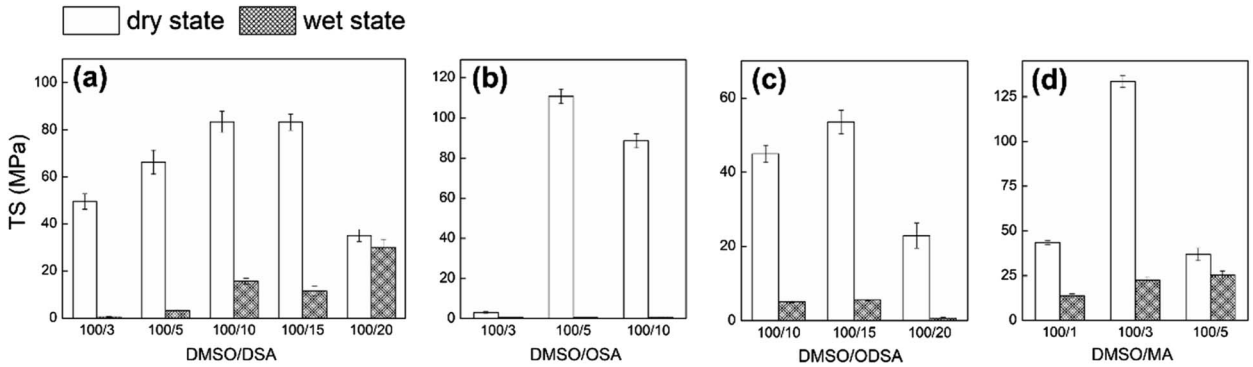

Fig. 2 TS of (a) 3%, 5%, 10%, 15% C12-BC, (b) 3%, 5%, 10% C8-BC, (c) 10%, 15%, 20% C18-BC, and (d) 1%, 3%, 5% C0-BC in dry and wet states at 70 °C for 5 min.

Table 2 DSS of anhydride modified films at 10 min–3 h

	Reaction time			
Sample	10 min	30 min	1 h	3 h
3% C0-BC	3	3	3	3
5% C8-BC	0.122	0.166	0.187	0.191
10% C12-BC	0.061	0.072	0.075	0.098
15% C18-BC	0.033	0.067	0.093	0.117

intercalation of hydrophobic groups destroyed the hydrogen bonds and decreased the dry TS of the film, the surface strengthening and the increased hydrophobicity significantly enhanced both the dry and wet TS, respectively. Late in the reaction, irregular fluctuations were observed in the mechanical strength of the modified films due to the side reactions including the solvent over-swelling and transesterification. Meanwhile, the wet TS decreased considerably and wet EAB increased because of the intercalation of water molecules into the polymer chains that acted as a plasticizing effect.

The finding that 10% C12-BC-30 min displayed the highest strength (dry TS = 124.3 ± 2.1 MPa, wet TS = 81.0 ± 1.7 MPa) might be due to the good balance between the solvent strengthening, esterification, and side reactions. The mechanical properties (dry and wet state) of 3% C0-BC-30 min were poorer than those of 5% C8-BC-30 min, 10% C12-BC, and 15% C18-BC, due to the shortly substituted chains from MA and high DSS of 3% C0-BC that provide relatively low surface hydrophobicity and dense crosslinking structure, causing the film to be fractured more easily under moisture conditions and limiting the film extension under tensile force, as revealed by the low TS (wet) and EAB (dry and wet) of 3% C0-BC (Fig. 3e and f). 3% C0-BC-1 h had a considerable decrease in dry EAB (3.8%) and dry TS (50 MPa) when compared with that of 3% C0-BC-30 min (dry state: TS = 90 MPa, EAB = 7.3%), which might have been caused

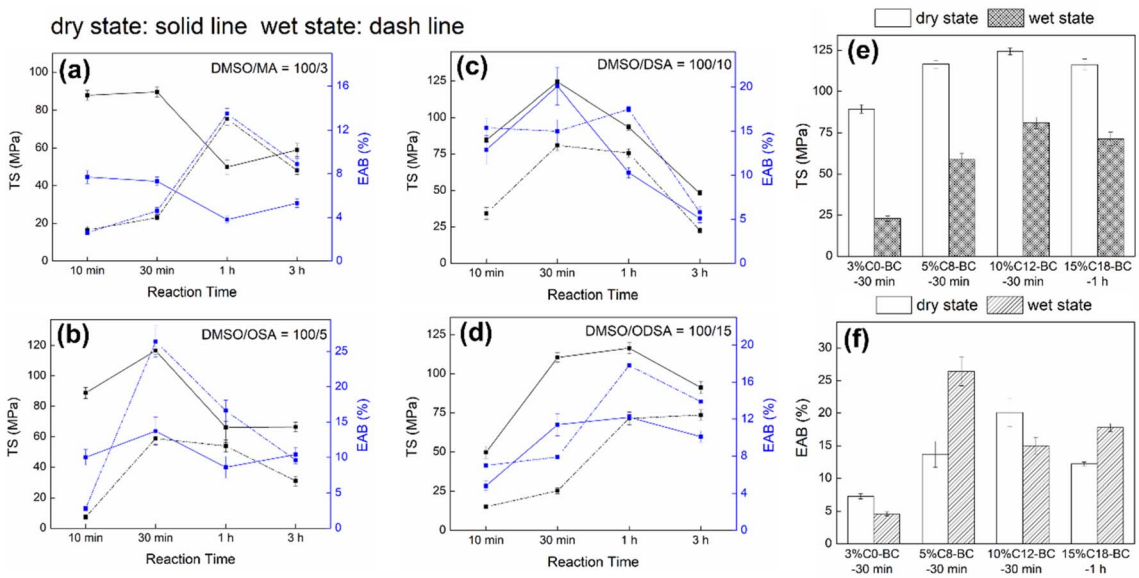

Fig. 3 TS and EAB of the (a) 3% C0-BC, (b) 5% C8-BC, (c) 10% C12-BC, and (d) 15% C18-BC films in dry and wet states from 10 min to 3 h. Optimal (e) TS and (f) EAB of the 3% C0-BC, 5% C8-BC, 10% C12-BC, and 15% C18-BC films in dry and wet states.

by the increasing crosslinking degree with extending reaction time that made the film stiffer. After immersing in water, owing to the plasticization effect of water that greatly reduced the stiffness of the film, the TS of 3% C0-BC-1 h increased from 50 MPa to 75 MPa.

Fourier-transform infrared spectroscopy (FTIR) results

Fig. 4 compares the FTIR spectra of the reference BC and the short- or long-chain anhydride modified films from 10 min to 3 h. The wide band between 3200 and 3500 cm^{-1} is assigned to the vibration of –OHs present in BC.[43] The peak at 2364–2369 cm^{-1} confirms the formation of an S–H bond between DMSO and BC,[44] and the low awt% of sulfur detected by EDS (Table S2†) verifies that only a small amount of DMSO was left on the surface. The intensifying peaks at 2960–2855 cm^{-1} in the spectra of 5% C8-BC-30 min–3 h and 15% C18-BC-1 h–3 h represent considerable increases in the C–H stretching vibrations of $–CH_3$ and $–CH_2$ derived from the grafted long aliphatic groups of OSA and ODSA (Fig. 4b and d), whereas no peak broadening was observed at 2960 cm^{-1} in the spectrum of 3% C0-BC-10 min–3 h (Fig. 4a) because no $–CH_3$ groups existed on the MA modified BC structure.[8,24,45,46] The appearance of a band at 1723–1729 cm^{-1} represents the stretching vibrations of the carbonyl group (C=O) from ester moieties, indicating esterification between the anhydride and BC.[11] The C=O peak of 3% C0-BC-10 min was significantly higher than that those of the long-chain anhydride modified films at 10 min, demonstrating the highest reactivity of MA that introduced significant C=O groups in a short reaction period, consistent with the DSS results presented above.

X-ray diffraction (XRD) results

Grafting of long-chain hydrophobic groups reduced the number of hydrogen bonds in BC films, resulting in a reduction in the CrI. The CrIs of the DMSO treated films were not obviously affected from 30 min to 1 h (Table 3). Instead, the CrIs of the anhydride modified films over the same time period were calculated in this study. The chain length and DSS were identified as the two main factors that affected the crystalline structure (Fig. S1,† Table 3). The CrIs of the modified films were all lower than that of the reference. The CrI of 3% C0-BC-30 min–1 h had the smallest CrI reduction of 0.66–6.8% due to the short alkyl groups grafted on the BC surface, which caused less disruption of the hydrogen bonds. 10% C12-BC had a small reduction in CrI of 5.7–10.2%, and 5% C8-BC had the largest reduction of 18.7–32.3%, which might be attributable to these films having a low and high DSS, respectively. The CrI of 15% C18-BC showed a relatively large reduction, 19.0–22.3%, which might have been due to the ultra-long alkenyl chain, which greatly disturbed the hydrogen-bonding between the inter- and intra-polymer chains.

Film microstructure results

As shown in Fig. 5a and b, the pristine BC film exhibited a highly porous structure with pore sizes of 50–270 nm. In comparison,

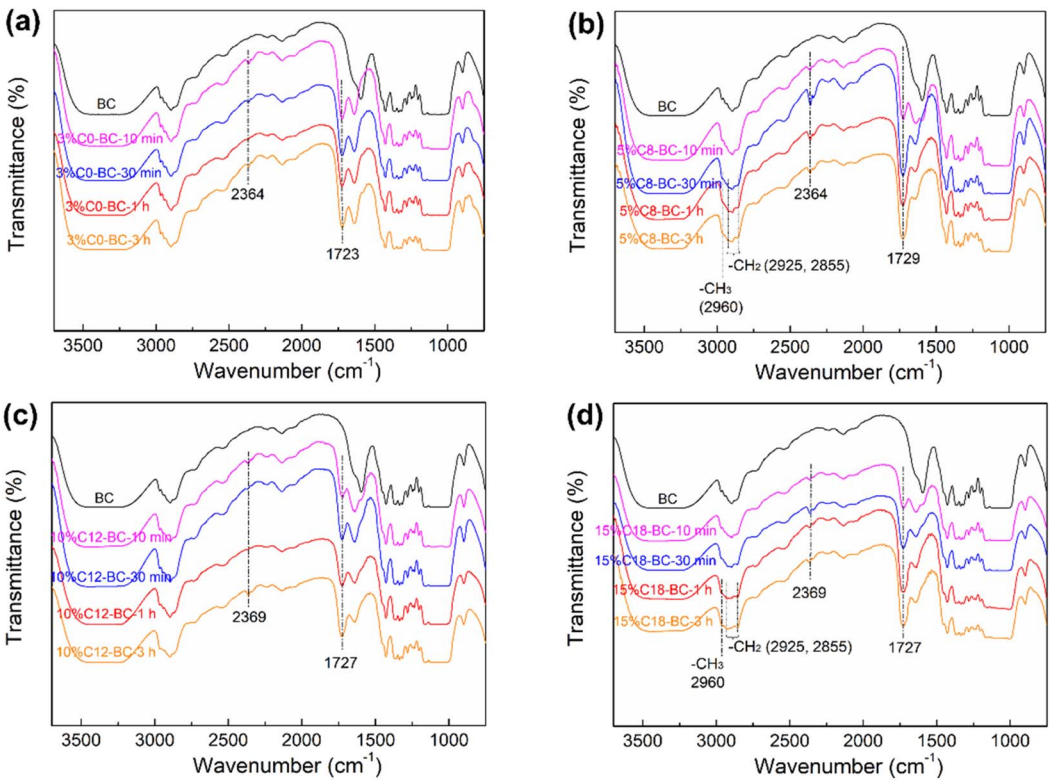

Fig. 4 FTIR spectra of the pristine BC and (a) 3% C0-BC, (b) 5% C8-BC, (c) 10% C12-BC, and (d) 15% C18-BC films from 10 min to 3 h.

Table 3 CrI of the pristine BC, 3% C0-BC, 5% C8-BC, 10% C12-BC, and 15% C18-BC films at 10 min–3 h

Sample	BC	DMSO-30 min	DMSO-1 h	3% C0-BC-30 min	3% C0-BC-1 h	5% C8-BC-30 min	5% C8-BC-1 h	10% C12-BC-30 min	10% C12-BC-1 h	15% C18-BC-30 min	15% C18-BC-1 h
CrI (%)	76.1	73.9	70.5	75.6	70.9	61.9	51.5	68.3	71.8	59.1	61.6

only a few small pores were observed on 3% C0-BC, proving that this film had a much denser surface morphology (Fig. 5c and d). Compared with the pristine BC film, 5% C8-BC and 15% C18-BC had smaller pores, while 10% C12-BC displayed no significant difference in pore size (Fig. 5e–j). The surface structure of 3% C0-BC-1 h (Fig. 5d) is denser than that of 10% C12-BC-1 h (Fig. 5h). It appeared that as the DSS of the modified film increased, the surface structure became denser. There were no visible differences in the cross-section morphologies of the pristine BC and 3% C0, 5% C8, 10% C12, and 15% C18-BC-1 h (Fig. S2a–d†). The near-surface cross-section of the film appeared not to have been affected by modification with OSA for 1 h (Fig. S2e and f†), although the surface morphology and CrI of 5% C8-BC-1 h were impacted visibly.

Water resistance properties

Esterification and crosslinking both enhance surface hydrophobicity and water-vapor resistance of the hydroxyl-rich biofilm.[47,48] As shown in Table S4† and Fig. 6, the unmodified BC film showed high hydrophilicity from the WCA measurements, and an obvious enhancement in WCA was realized for the modified films (Fig. 6a and b). The WCA of 3% C0-BC was lower than that of 5% C8-BC, 10% C12-BC, and 15% C18-BC, due to the shortly substituted chains from MA that provided relatively low surface hydrophobicity. The highest WCA (104°) was observed for 15% C18-BC-1–3 h, as ODSA had the longest substituted alkenyl chain with the highest hydrophobicity. While the pristine BC film quickly swelled and fragmented in water, the modified BC films absorbed much less water. Their WS ratios are displayed in Fig. 6c, and are postulated to have been determined by the chain length and crosslinking degree of the modified films. The WS ratios of the modified films from 10 min to 1 h in the order from lowest to highest are as follows: 3% C0-BC < 15% C18-BC < 5% C8-BC < 10% C12-BC. The reason why the WS ratio of 3% C0-BC was superior to that of the long-chain alkenyl anhydride modified BC is the much denser crosslinking structure formed on the surface of 3% C0-BC that made it more effective to block the penetration of water molecules to the inner structure.[8] The finding that 15% C18-BC displayed a lower WS ratio than that of 10% C12-BC can be attributed to the ultralong substituted alkenyl chain of ODSA and the low DSS of 10% C12-BC. The finding that the WS ratio of 5% C8-BC-3 h was lower than that of 15% C18-BC-3 h might have been explained by the higher DSS and crosslinking degree of the former film. As seen in Fig. 6d, 5% C8-BC-3 h and 15% C18-BC-1 h exhibited the most reduced WVP by 59.5% and 66.9%, respectively, owing to the higher DSS of 5% C8-BC-3 h and the ultra-long alkenyl chain of ODSA, respectively. The finding that 3% C0-BC displayed the lowest reduction in WVP by 8.7–28.9% was attributable to the poor WVP imparted by the short alkyl chains.

The WVP of the BC film was further reduced by 84% at a loading ratio of 10% OSA and after reaction for 1 h, whereas increasing the OSA ratio to 15% only reduced the WVP by 66% (3 h) (Table S5,† Fig. 7a and b). In addition, 10% C8-BC showed a slight reduction in mechanical strength (Table S6,† Fig. 7c)

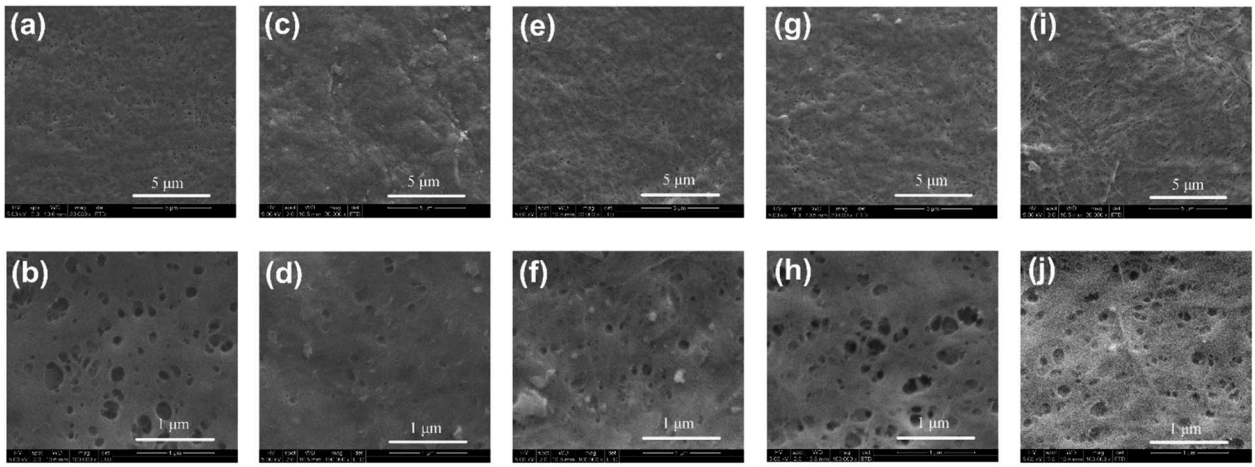

Fig. 5 SEM images (surface) of the (a and b) pristine BC, (c and d) 3% C0-BC-1 h, (e and f) 5% C8-BC-1 h, (g and h) 10% C12-BC-1 h, and (i and j) 15% C18-BC-1 h films at 20 000× and 100 000× magnification, respectively.

compared with 5% C8-BC, and a further decrease in strength was observed in 15% C8-BC (Table S7,† Fig. 7d), indicating that above a certain ratio in DMSO, OSA could hinder the reaction and reduce the water vapor barrier and mechanical strength of the films.[49] As shown in the FTIR spectra of 10% C8-BC and 15% C8-BC (Fig. 7e and f), the higher C=O intensity of the former at 10 min revealed a higher DSS, which was also supported by the higher C=O intensity of 10% C8-BC-30 min at 1711–1740 cm^{-1} than of 15% C8-BC-30 min. This difference can be attributed to the higher number of pendant –COOHs derived from the ring-opened OSA due to the higher DSS of 10% C8-BC-30 min.[50]

Antimicrobial properties

Antimicrobial function is critical for food packaging materials to minimize food spoiling caused by harmful microbes. The

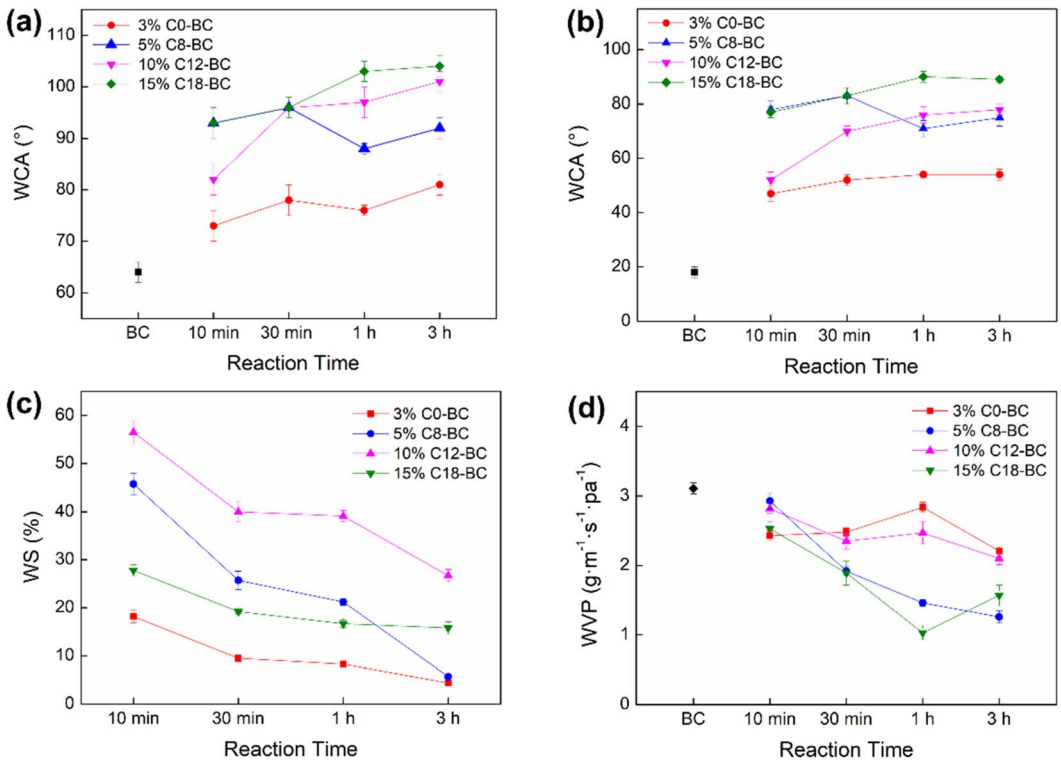

Fig. 6 (a) WCA (1 s), (b) WCA (5 min), (c) WS ratio, and (d) WVP of the 3% C0-BC, 5% C8-BC, 10% C12-BC, and 15% C18-BC films from 10 min to 3 h.

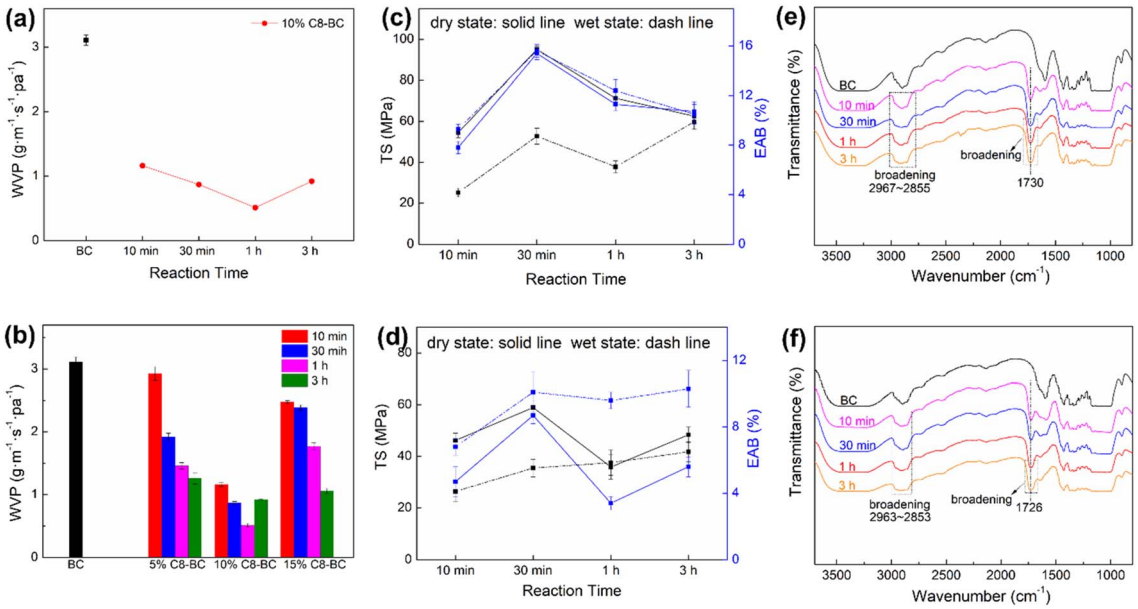

Fig. 7 (a) WVP of the 10% C8-BC-10 min–3 h films. (b) Comparison of WVP of the pristine BC and 5, 10, and 15% C8-BC-10 min–3 h films. TS and EAB in the dry (solid line) and wet states (dashed line) of (c) the 10% C8-BC-10 min–3 h and (d) 15% C8-BC-10 min–3 h films. FTIR spectra of the (e) 10% C8-BC and (f) 15% C8-BC films at 10 min–3 h.

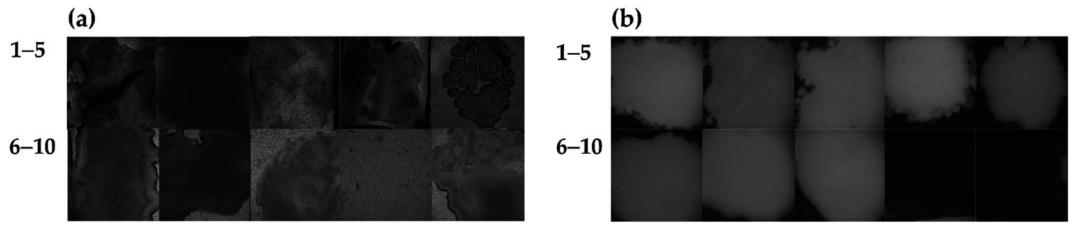

Fig. 8 Microscopic images of (a) *S. aureus* and (b) *E. coli* treated samples: (1–3) 3% C0-BC-10 min, 30 min, 1 h; (4–6) 5% C8-BC-30 min, 1 h, 3 h; (7–10) 10% C8-BC-10 min, 30 min, 1 h, 3 h.

hydrophobicity of the film was reported to be an important factor that contributes to a high antimicrobial effect (AE) on a biopolymer film surface.[51] As shown in Fig. 8, whereas the surfaces of 3% C0-films (samples 1–3) and 5% C8-BC films (samples 4–6) were almost covered with bacterial colonies, 10% C8-BC-1 h (sample 9) displayed the highest AE against both *E. coli* (white dots) and *S. aureus* (dark dots), implying its effectiveness for preventing the attachment and growth of these bacteria. The AE of 10% C8-BC-1 h was distinctly higher than that of 3% C0-BC, mainly because the former with long octenyl groups had a strong hydrophobic interaction with the bacterial cell wall proteins that effectively destroys the cell wall and cell membranes, consequently causing the leakage of intracellular proteins/nucleic acids and eventually the cell death.[32,51,52]

Oxygen barrier properties

As shown in Table 4, 3% C0-BC-30 min–1 h had a much stronger oxygen barrier than the other modified films, which can be attributed to the significantly higher CrIs of 3% C0-BC-30 min and 3% C0-BC-1 h (Table 3). Based on this, it is conjectured that the OTR of a cellulose film may be directly influenced by its crystallinity. The films modified by the long-chain octenyl anhydride OSA had a much weaker oxygen barrier than the other films, which is attributable to their largely decreased CrI

Table 4 OTR of the pristine BC, 3% C0-BC, 5, and 10% C8-BC films at 30 °C, 95% RH at 10 min–3 h

		3% C0-BC				5% C8-BC				10% C8-BC			
Sample	BC	10 min	30 min	1 h	3 h	10 min	30 min	1 h	3 h	10 min	30 min	1 h	3 h
OTR (g m^{-2} h^{-1})	4.35 ± 0.42	2.88 ± 0.22	0.69 ± 0.11	0.53 ± 0.15	3.65 ± 0.24	2.71 ± 0.20	3.10 ± 0.18	3.18 ± 0.19	3.25 ± 0.25	2.95 ± 0.15	3.48 ± 0.31	4.83 ± 0.36	3.13 ± 0.26

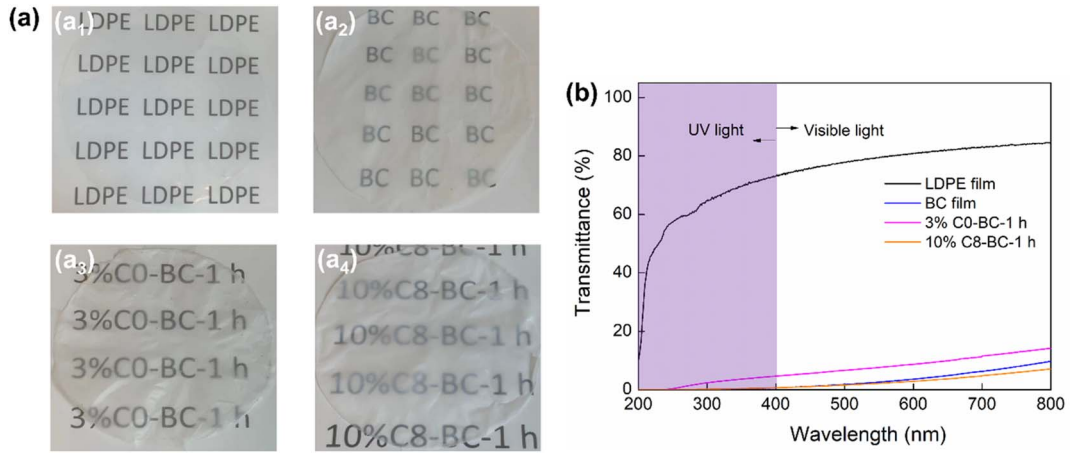

Fig. 9 (a) Photographs and (b) UV-vis spectra of the LDPE, pristine BC, 3% C0-BC-1 h, and 10% C8-BC-1 h films.

(Table 3) caused by the insertion of long alkenyl chains that greatly destroyed the hydrogen bonding of the film so that providing more free volume for oxygen molecules to pass through.[53,54] The reason why pristine BC and 3% C0-BC-10 min films displayed a higher OTR could be explained by their greatly decreased water vapor and oxygen barrier under high RH that facilitated the oxidation of reduced iron powder.

Visible and ultraviolet (UV) light barrier properties

As shown in Fig. 9, the LDPE film displayed high visible light transmittance but poor UV-shielding properties, while the pristine BC, 3% C0-BC-1 h and 10% C8-BC-1 h films were all semi-transparent and showed high UV light shielding over the UV-vis spectrum between 200 and 400 nm. Furthermore, 10% C8-BC-1 h displayed lower visible light transmittance than did 3% C0-BC-1 h and the pristine BC films, which might have been due to effective blocking of visible light by the long substituted chains. It is speculated that the less porous surface structure of 3% C0-BC-1 h could cause less surface scattering of light, resulting in its higher transparency than the pristine BC film.

Strawberry quality during storage

Water vapor and oxygen are the two main factors that influence the quality of packaged fruits, including their appearance and texture over time, due to microbial action, oxidation, and respiration, which result in corruption and loss of nutrition.[37] The shelf-lives of strawberries under five preservation conditions were evaluated, as shown in Fig. 10. After storage for 9 d,

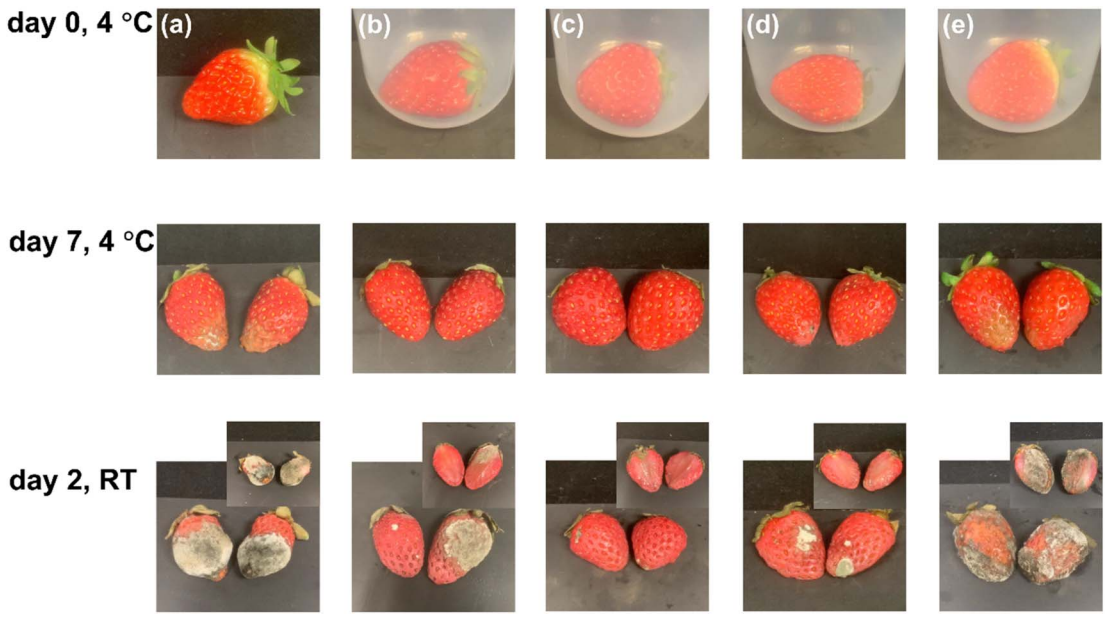

Fig. 10 The surfaces and inner structure of strawberries (a) left uncovered or covered with (b) the pristine BC film, (c) 3% C0-BC-1 h, (d) 10% C8-BC-1 h, and (e) LDPE for storage durations of 0 d and 7 d at 4 °C, 40% RH, followed by storage at RT (24 °C, 55% RH) for 2 d.

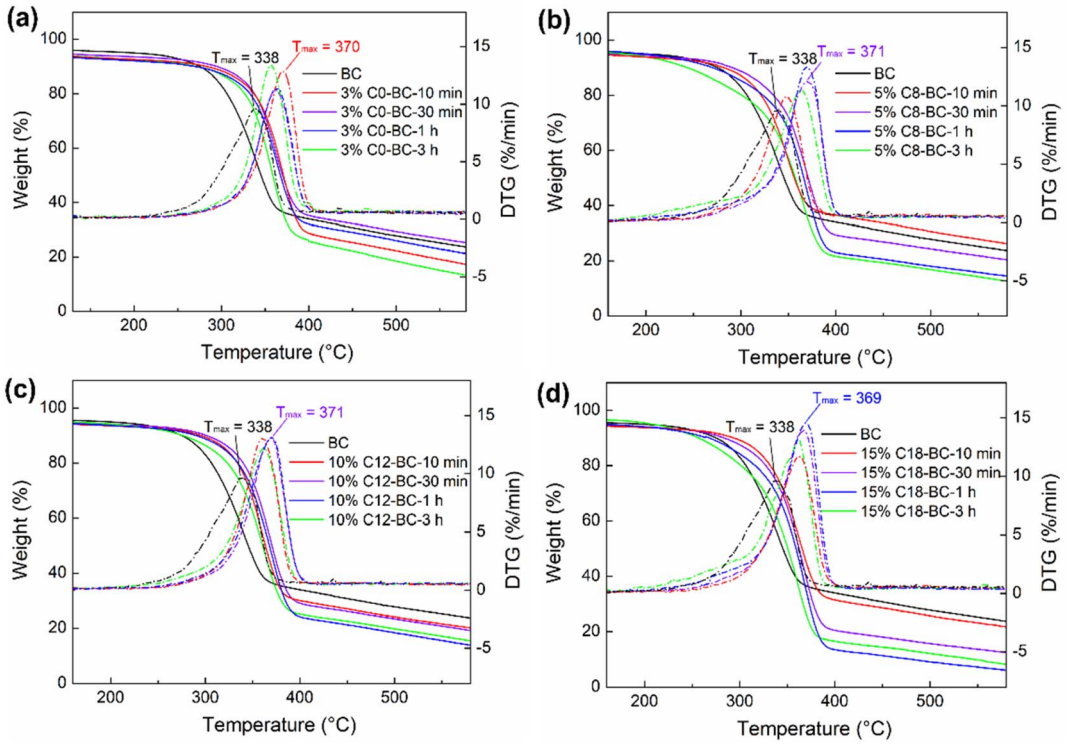

Fig. 11 Thermogravimetric analysis and DTG of the pristine BC and (a) 3% C0-BC, (b) 5% C8, (c) 10% C12, and (d) 15% C18-BC films at 10 min–3 h.

surface observation revealed that the uncovered and LDPE covered strawberries had the greatest loss of freshness, as revealed by serious yellowing, mold growth, and shrinkage on the surfaces and inner structures of the samples (Fig. 10a and e). The original BC film covered sample also exhibited obvious mold growth after storage (Fig. 10b), due to the poor oxygen barrier of the BC and LDPE films, which led to ascorbic acid oxidation and microorganism growth on the fruit tissue.[16,55] In comparison, the highest freshness was observed on the sample covered with 3% C0-BC-1 h after 7 d in a refrigerator and 2 d at RT, attributable to 3% C0-BC-1 h having the lowest OTR (Table 4), although slight mold growth was observed (Fig. 10c). More mold growth happening to 10% C8-BC-1 h covered strawberry (Fig. 10d) compared with the 3% C0-BC-1 h covered one was attributable to the much poorer oxygen barrier of the former (Table 4).

The strawberries were also weighed after 7 d to determine the weight loss after storage (Table S8†), which resulted from water evaporation to the confined space and then to the air. The LDPE covered samples lost only 7.9% of the initial weight, and a visible amount of water was retained in the LDPE covered bottle (Fig. S3†) due to the excellent water vapor resistance of LDPE, which strongly prevented water vapor transmission through the film. The 10% C8-BC-1 h covered strawberry lost 9% of its weight, while that covered with 3% C0-BC-1 h lost 16% of its weight. This difference was attributable to the significantly higher water vapor barrier of the former film (Fig. 7a). It is likely that the achievement of both high water vapor and oxygen barrier properties in a packaging film can allow the simultaneous repression of microbe growth on and moisture loss from fresh fruits/vegetables, thus significantly extending their shelf-lives. Accordingly, further exploration of the design of new protocols based on this surface modification strategy is needed.

Thermal properties

Esterification and solvent over-swelling effect decrease the thermal stability of the modified films, while the crosslinking reaction increases it.[56] Table S9† and Fig. 11 display the T_{max} values of the pristine and modified BC films. The cyclic anhydride modified BC films showed obvious enhancements in thermal stability: the highest T_{max} increased to approximately 370 °C for 3% C0-BC-10 min, 5% C8-BC-30 min, 10% C12-BC-30 min, and 15% C18-BC-1 h, compared with 338 °C for the pristine BC. Additionally, 3% C0-BC reached its T_{max} in 10 min while the other modified films reached their T_{max} in 30 min–1 h, attributable to the highest reactivity of MA enabling a large number of –COOHs to be involved in early participation in the crosslinking reaction. The decrease in T_{max} over time can be explained by the solvent over-swelling effect, such that the depth of the film surface gradually increased with swelling and caused a decrease in thermal stability. A previous study reported that a BC film totally regenerated from *N*-methylmorpholine *N*-oxide showed a considerable reduction in thermal stability compared with the original BC film, indicating that a high level of regeneration on a film could decrease its thermal stability.[27]

Biodegradation analysis

Easy biodegradability in nature is a highly valued characteristic of a food packaging material. The pristine BC, 3% C0-BC-1 h,

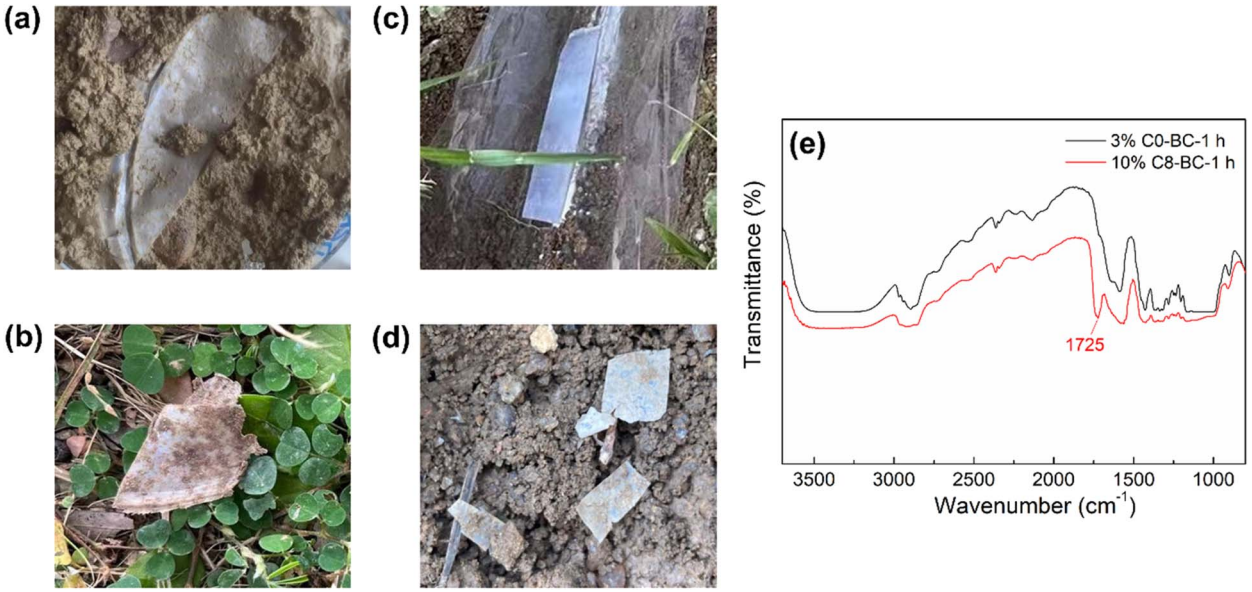

Fig. 12 Biodegradability test of the 3% C0-BC-1 h film at (a) 0 d and (b) 10 d and the 10% C8-BC-1 h film at (c) 0 d and (d) 10 d in soil. (e) FTIR spectra of the 3% C0-BC-1 h and 10% C8-BC-1 h films after biodegradation in soil for 10 d.

and 10% C8-BC-1 h films were buried in soil for 1 month, after which the extent of biodegradation was studied according to the weight loss test and FTIR results. While the pristine BC film had totally biodegraded after 10 d, the surface modified films, namely 3% C0-BC-1 h and 10% C8-BC-1 h, had cracked and lost 74.0% and 49.7% of their weight after 10 d (Fig. 12a–d), respectively, and had totally biodegraded after 1 month. The above results demonstrated that the cyclic anhydride modified films prepared in this study could easily biodegrade in natural soil, and that the short-chain modified films degraded faster than the long-chain modified ones. The FTIR results (Fig. 12e) also verified that the ester groups on 3% C0-BC-1 h were more easily eliminated than those on 10% C8-BC-1 h when compared with the FTIR spectra of the unburied films (Fig. 4a and 7e),[20,57] which could be explained by the much higher water vapor resistance of the latter film that prevented hydrolyzation attack at the ester groups by the enzyme esterase in soil.[16] Those results reveal the various biodegradation rates of modified films bearing different hydrophobic chains, and their easy biodegradation properties in natural soil. The surface modification strategy can be the reason for the fast biodegradation rate as only the film surface has been hydrophobically modified while the inner structure was still hydrophilic, demonstrating the great promise of BC as a substrate and cyclic anhydrides as surface modifiers at a low loading ratio in DMSO in the development of easily biodegradable food packaging films.

Conclusions

Using four cyclic anhydrides as the acylants and DMSO as the solvent, alkyl moieties with different lengths (C0–C18) were successfully introduced onto the surfaces of a premade BC film. The loading ratio of each anhydride in DMSO (3–15%) and the reaction period (10 min–3 h) were optimized to achieve modified films with good mechanical and water vapor, oxygen, and foodborne pathogenic bacterial barrier properties. The degree of surface grafting was confirmed by the results of FTIR spectroscopy and SEM EDS. Compared with the other long-chain alkenyl anhydride-modified films, 3% C0-BC reached the lowest mechanical strength and displayed the poorest water vapor barrier. 10% C12-BC-30 min achieved the highest dry TS (>120 MPa) and wet TS (> 80 MPa) in only 30 min, while 15% C18-BC-3 h reached the highest WCA (104°). The lowest WVP (reduced by 84%), best antimicrobial effect and highest moisture retention from strawberries were realized using 10% C8-BC-1 h as the packaging film. 3% C0-BC-1 h, which had a well-preserved CrI, displayed the highest oxygen barrier and fruit preservation performance, demonstrating the effectiveness of a crystalline film with a high oxygen barrier in inhibiting microorganism growth on fruits. Furthermore, all of the anhydride modified films showed visible improvements in thermal stability by around 32 °C and good biodegradation rate (100% biodegradation in 1 month) in soil. As a result, those biobased films display high potential in replacement of the widely used petrochemical plastic-based food packaging materials as high water and oxygen vapor barrier, strong and biodegradable films to greatly extend shelf-lives of foods and effectively relieve the white pollution in the environment.

Author contributions

Zhuolun Jiang: methodology, conceptualization, data curation, formal analysis, writing – original draft, writing – review & editing. Ka Man Cheung: data curation; To Ngai: investigation, project administration, writing – review & editing, supervision, funding acquisition. All authors have read and agreed to the published version of the manuscript.

Conflicts of interest

There are no conflicts to declare.

Acknowledgements

The financial support of the Research Matching Grant Scheme at CUHK (8601309) is acknowledged. Thanks for the kind support from Prof. Yilin Wu and Xuequan Lai from the Department of Physics, CUHK, who provided the modified Gram-negative bacteria *Escherichia coli* and helped us with the antimicrobial test and imaging work. Thanks for the support from Prof. Xiao Yang and Kendra Li from Department of Microbiology, CUHK, who provided us with the Gram-positive bacteria *Staphylococcus aureus*.

References

1 R. Geyer, J. R. Jambeck and K. L. Law, *Sci. Adv.*, 2017, **3**, e1700782.
2 M. Larrain, P. Billen and S. Van Passel, *Waste Manage.*, 2022, **153**, 355–366.
3 Y. Liu, S. Ahmed, D. E. Sameen, Y. Wang, R. Lu, J. Dai, S. Li and W. Qin, *Trends Food Sci. Technol.*, 2021, **112**, 532–546.
4 D. Khodaei, C. Álvarez and A. M. Mullen, *Polymers*, 2021, **13**, 2561.
5 A. Surendren, A. K. Mohanty, Q. Liu and M. Misra, *Green Chem.*, 2022, **24**, 8606–8636.
6 Q.-F. Guan, Z.-C. Ling, Z.-M. Han, H.-B. Yang and S.-H. Yu, *Matter*, 2020, **3**, 1308–1317.
7 T. Aditya, J. P. Allain, C. Jaramillo and A. M. Restrepo, *Int. J. Mol. Sci.*, 2022, **23**, 610.
8 Y. Sun, D. Chen, Y. Li, S. Sun, J. Zheng, J. Cui, G. Wang, L. Zheng, Y. Wang and H. Zhou, *Carbohydr. Polym.*, 2021, **270**, 118359.
9 D. N. Phan, M. Q. Khan, N. T. Nguyen, T. T. Phan, A. Ullah, M. Khatri, N. N. Kien and I. S. Kim, *Carbohydr. Polym.*, 2021, **252**, 117175.
10 Y. Habibi, *Chem. Soc. Rev.*, 2014, **43**, 1519–1542.
11 Y.-t. Song, J.-r. Qi, X.-q. Yang, J.-s. Liao, Z.-w. Liu and C.-w. Ruan, *Food Hydrocolloids*, 2022, **132**, 107832.
12 P. V. Navya, V. Gayathri, D. Samanta and S. Sampath, *Int. J. Biol. Macromol.*, 2022, **220**, 435–461.
13 W. Liu, K. Liu, H. Du, T. Zheng, N. Zhang, T. Xu, B. Pang, X. Zhang, C. Si and K. Zhang, *Nano-Micro Lett.*, 2022, **14**, 104.
14 H. B. Yang, Z. X. Liu, C. H. Yin, Z. M. Han, Q. F. Guan, Y. X. Zhao, Z. C. Ling, H. C. Liu, K. P. Yang, W. B. Sun and S. H. Yu, *Adv. Funct. Mater.*, 2021, 2111713.
15 P. Cazón and M. Vázquez, *Food Hydrocolloids*, 2021, **113**, 106530.
16 Z. Jiang, Z. Shi, K. M. Cheung and T. Ngai, *ACS Sustainable Chem. Eng.*, 2023, **11**, 2486–2498.
17 Z. Wan, L. Wang, L. Ma, Y. Sun and X. Yang, *ACS Biomater. Sci. Eng.*, 2017, **3**, 1595–1604.
18 F. Rol, M. N. Belgacem, A. Gandini and J. Bras, *Prog. Polym. Sci.*, 2019, **88**, 241–264.
19 S. P. Bangar, M. M. Harussani, R. A. Ilyas, A. O. Ashogbon, A. Singh, M. Trif and S. M. Jafari, *Food Hydrocolloids*, 2022, **130**, 107689.
20 Q. Chen, C. Chang and L. Zhang, *Carbohydr. Polym.*, 2021, **269**, 118315.
21 K. Zeng, J. Gu and C. Cao, *ACS Appl. Mater. Interfaces*, 2020, **12**, 18987–18996.
22 C. Jo, B. Rukmanikrishnan, P. D. S, S. Ramalingam and J. Lee, *ACS Sustainable Chem. Eng.*, 2021, **9**, 13653–13662.
23 B. Hutton-Prager, K. Adenekan, M. Sypnewski, A. Smith, M. Meadows and C. Calicdan, *Cellulose*, 2021, **28**, 1633–1646.
24 L. C. Tomé, M. G. Freire, L. P. N. Rebelo, A. J. D. Silvestre, C. P. Neto, I. M. Marrucho and C. S. R. Freire, *Green Chem.*, 2011, **13**, 2464–2470.
25 K. Huang and Y. Wang, *Curr. Opin. Food Sci.*, 2022, **43**, 7–17.
26 U. Ratanakamnuan, D. Atong and D. Aht-Ong, *Carbohydr. Polym.*, 2012, **87**, 84–94.
27 M. Ul-Islam, S. Khan, M. W. Ullah and J. K. Park, *Int. J. Biol. Macromol.*, 2019, **137**, 247–252.
28 M. Lakovaara, J. A. Sirviö, M. Y. Ismail, H. Liimatainen and R. Sliz, *Cellulose*, 2021, **28**, 5433–5447.
29 Z. Yao, S. Mi, B. Chen, F. Liu, H. Na and J. Zhu, *ACS Sustainable Chem. Eng.*, 2022, **10**, 17327–17335.
30 G. Tedeschi, J. J. Benitez, L. Ceseracciu, K. Dastmalchi, B. Itin, R. E. Stark, A. Heredia, A. Athanassiou and J. A. Heredia-Guerrero, *ACS Sustainable Chem. Eng.*, 2018, **6**, 14955–14966.
31 M. C. Sweedman, M. J. Tizzotti, C. Schafer and R. G. Gilbert, *Carbohydr. Polym.*, 2013, **92**, 905–920.
32 N. N. Shah, N. Soni and R. S. Singhal, *Int. J. Biol. Macromol.*, 2018, **107**, 2224–2233.
33 H. Sehaqui, T. Zimmermann and P. Tingaut, *Cellulose*, 2014, **21**, 367–382.
34 J. Antoniou, F. Liu, H. Majeed and F. Zhong, *Food Hydrocolloids*, 2015, **44**, 309–319.
35 B. Dhuiège, G. Pecastaings and G. Sèbe, *ACS Sustainable Chem. Eng.*, 2019, **7**, 187–196.
36 L. Cao, G. Sun, C. Zhang, W. Liu, J. Li and L. Wang, *J. Agric. Food Chem.*, 2019, **67**, 2066–2074.
37 X. Liu, Y. Xu, W. Liao, C. Guo, M. Gan and Q. Wang, *Food Packag. Shelf Life*, 2023, **35**, 101006.
38 N. Goudar, V. N. Vanjeri, S. Dixit, V. Hiremani, S. Sataraddi, T. Gasti, S. K. Vootla, S. P. Masti and R. B. Chougale, *Int. J. Biol. Macromol.*, 2020, **158**, 139–149.
39 B. Lindman, B. Medronho, L. Alves, C. Costa, H. Edlund and M. Norgren, *Phys. Chem. Chem. Phys.*, 2017, **19**, 23704–23718.
40 P. Uschanov, L.-S. Johansson, S. L. Maunu and J. Laine, *Cellulose*, 2011, **18**, 393–404.
41 W. Li, S. Wang, W. Wang, C. Qin and M. Wu, *Cellulose*, 2019, **26**, 3271–3284.
42 C. S. R. Freire, A. J. D. Silvestre, C. P. Neto, M. N. Belgacem and A. Gandini, *J. Appl. Polym. Sci.*, 2006, **100**, 1093–1102.
43 S. Mohammadalinejhad, H. Almasi and M. Moradi, *Food Control*, 2020, **113**, 107169.
44 N. Deepa, K. Aanantharaj, A. Vimala Juliet, R. Sujith and J. Sherine, *Appl. Nanosci.*, 2021, **11**, 2337–2346.

45 S. L. Balasubramaniam, A. S. Patel and B. Nayak, *Food Packag. Shelf Life*, 2020, **26**, 100587.
46 R. M. Ribeiro-Viana, P. C. Faria-Tischer and C. A. Tischer, *Carbohydr. Polym.*, 2016, **148**, 21–28.
47 E. Olsson, M. S. Hedenqvist, C. Johansson and L. Jarnstrom, *Carbohydr. Polym.*, 2013, **94**, 765–772.
48 T. Zheng, X. Yu and S. Pilla, *Carbohydr. Polym.*, 2017, **157**, 1333–1340.
49 Q. Xiao, H. Weng, G. Chen and A. Xiao, *Food Chem.*, 2019, **279**, 30–39.
50 O. Gershevitz and C. N. Sukenik, *J. Am. Chem. Soc.*, 2003, **126**, 482–483.
51 A. Venkateshaiah, K. Havlicek, R. L. Timmins, M. Rohrl, S. Waclawek, N. H. A. Nguyen, M. Cernik, V. V. T. Padil and S. Agarwal, *Carbohydr. Polym.*, 2021, **266**, 118126.
52 V. V. Padil, C. Senan and M. Cernik, *J. Agric. Food Chem.*, 2015, **63**, 3757–3765.
53 K. Syverud and P. Stenius, *Cellulose*, 2009, **16**, 75–85.
54 C. Aulin, M. Gallstedt and T. Lindstrom, *Cellulose*, 2010, **17**, 559–574.
55 X. Zhou, R. Cheng, B. Wang, J. Zeng, J. Xu, J. Li, L. Kang, Z. Cheng, W. Gao and K. Chen, *Carbohydr. Polym.*, 2021, **251**, 117117.
56 K. Y. Lee, F. Quero, J. J. Blaker, C. A. S. Hill, S. J. Eichhorn and A. Bismarck, *Cellulose*, 2011, **18**, 595–605.
57 K. Sakai, T. Yamauchi, F. Nakasu and T. Ohe, *Biosci., Biotechnol., Biochem.*, 1996, **60**, 1617–1622.